Special Feature: CAE and Simulation

Research Report

Phase-field Models for Microstructural Characterization of Platinum-based Alloy Nanoparticles

Shunsuke Yamakawa, Ryoji Asahi and Toshiyuki Koyama

Report received on Oct. 29, 2014

ABSTRACT The phase-field method based on the formulation of free energy functions is a numerical simulation technique that can be used to investigate the microstructural formation process of an inorganic material. The objective of the present study is to construct an effective phase-field model to describe the compositional variation within a binary alloy nanoparticle. The model provides information on crucial factors that affect the internal structure of a transition metal-platinum alloy nanoparticle serving as the cathode electrocatalyst of a polymer electrolyte fuel cell. We use the phase-field model to investigate the radial distributions of the phase state and the atomic compositions of CrPt, FePt, CoPt, NiPt, CuPt, PdPt, IrPt, and AuPt nanoparticles with diameters smaller than 10 nm. The results reveal that the compositional variation within a single particle depends on the balance between the atomic interactions within particles and the surface energy, and that the specific equilibrium structures vary significantly with the alloy combination. To reduce excessive surface segregation and prevent instability in the alloy system, it is possible to take advantage of the formation of ordered phases.

KEYWORDS Platinum Catalyst, Nanoparticle, Surface Segregation, Ordered Phase, Phase-field Method, CALPHAD

1. Introduction

Computational modeling studies are useful for elucidating the driving forces behind microstructure formation and predicting the resultant microstructures. Methods of simulating the material structure at the nanometer to micrometer scale can be roughly classified into two categories: (i) methods that simulate the temporal evolution of the microstructure by calculating the atomic motion directly, and (ii) methods that describe the microstructural evolution by calculating the transform of a set of spatially dependent field variables. Molecular dynamics and Monte Carlo methods based on a classical or first-principles potential typically belong to the first group. The phase-field method, which is a continuum model belonging to the second group and obeys local thermodynamic equilibrium, has been widely used since the 1980s to study a variety of microstructure formations such as dendritic growth, spinodal decomposition, and grain growth.[1,2] In the present study, we describe a phase-field model for the prediction of the microstructures of a transition metal-platinum (TM-Pt) binary alloy nanoparticle used as a cathode electrocatalyst, with an eye toward improving the performance of polymer-electrolyte fuel cells (PEFCs).

Driven by immediate demands for alternative fuel resources that can replace existing fossil fuels, extensive studies have been conducted to develop new, clean, and efficient carriers of energy. One interesting approach to improving the fuel efficiency and suppressing carbon dioxide emissions in vehicles is the application of PEFCs.[3] As shown in **Fig. 1**,[4] simultaneous processes occur in a PEFC, from the anode across the electrolyte to the cathode. One of the key challenges in achieving high-performance fuel cell systems is to develop efficient and reliable electrocatalysts as an alternative to expensive pure platinum for the oxygen reduction reaction (ORR) at the cathode. To this end, TM-Pt alloy nanoparticles have been studied intensively;[5] however, during the heat-treatment, which is a part of the nanoparticle synthesis process, compositional differences are often induced between the alloy's nanoparticle and normal bulk material[6] and between the particle surface and the particle interior.[7] These segregations in the TM-Pt binary alloy nanoparticle affect the catalytic activities

of the alloy, and thus need to be optimized.[8]

The objective of the present study is to construct an effective phase-field model to describe the compositional variation and phase transformation within a single catalyst particle of a TM-Pt binary alloy.[9,10] To verify the accuracy of this simulation, the model is first compared with experimental and other simulation results for the phase transformations in FePt nanoparticles. Next, the radial distribution of the phase state and the atomic compositions of CrPt, FePt, CoPt, NiPt, CuPt, PdPt, IrPt, and AuPt nanoparticles are investigated in order to obtain the general attributes of the surface segregation of an alloy nanoparticle in terms of the alloying combination, particle size, and heat-treatment temperature. These results elucidate how the composition of a single particle varies with the alloy combination, particle size, and heat-treatment temperature, leading to an understanding of alloy nanoparticle design.

2. Computational Methods

2. 1 Gibbs Free Energy Formulas

In the phase-field method, the conservative variables, which characterize the atomic concentrations, and the non-conservative variables, which characterize the structural heterogeneities, are defined as the field variables in the simulation area. In the present study, three types of field variables pertaining to the atomic concentration, c, long-range ordering (LRO), s, and phase transition, θ, between solid and liquid were introduced. We described the total free energy, G_{sys}, of the simulated system using these variables in the following form:

$$G_{sys} = \int [h(\theta)G_{chem}^{(S)} + (1-h(\theta))G_{chem}^{(L)} + W\theta(1-\theta) + \frac{1}{2}\sum_{i=1}^{n}\kappa_i(\nabla c_i)^2 + h(c)\frac{\kappa_s}{2}\sum_{i=1}^{3}(\nabla s_i)^2 + \frac{\kappa_\theta}{2}(\nabla\theta)^2]d\mathbf{r}, \quad (1)$$

$$h(x) = x^3(6x^2 - 15x + 10), \quad (2)$$

$$c = \sum_{i=1}^{n-1} c_i, \quad (3)$$

where the superscripts (S) and (L) indicate the solid and liquid phases, respectively; the variable c_i, the atomic concentration of component i, takes values between 0 and 1 normalized with respect to the maximum concentration; the variable s_i is defined later in Eq. (8); the variable θ is defined as the phase-field parameter so that θ values of 0 and 1 correspond to the liquid and solid phases, respectively; $G_{chem}^{(S)}$ and $G_{chem}^{(L)}$ are the bulk chemical free energy functions of the solid and liquid phases, respectively; W is the interfacial energy barrier between the solid and liquid phases; κ_i, κ_s and κ_θ are the gradient energy coefficients. Here, the binary TM-Pt alloy system is represented by a three-component setup ($n=3$): TM (component 1), Pt (component 2), and the vacancy, Va (component 3). The $G_{chem}^{(S)}$ and $G_{chem}^{(L)}$ for the disordered state were estimated under the assumption that the thermodynamic fields are spatially uniform and can be approximated

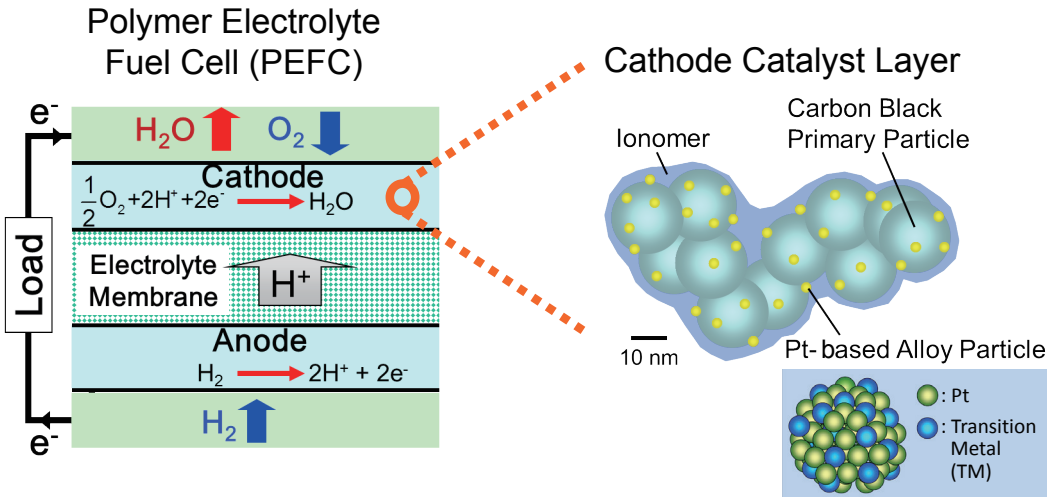

Fig. 1 Schematic illustrations of a PEFC system and an electro-catalyst supported on a carbon substrate.

by a regular solution model:[11]

$$G_{\mathrm{chem}}^{\mathrm{dis\_}(k)} = \sum_{i=1}^{n-1} c_i {}^{\circ}G_i^{(k)} + \sum_{i=1}^{n-1}\sum_{j=2,j>i}^{n} L_{ij}^{(k)} c_i c_j + RT\sum_{i=1}^{n} c_i \ln c_i , \quad k = \mathrm{S\ or\ L} , \tag{4}$$

where ${}^{\circ}G_i^{(k)}$ is the Gibbs formation energy of the pure element i in phase k, $L_{ij}^{(k)}$ is the binary interaction parameter, and R and T are the gas constant and absolute temperature, respectively. In the case of the ordered solid state, there is a contribution from long-range ordering, $\Delta G^{(\mathrm{ord})}$:

$$G_{\mathrm{chem}}^{(\mathrm{S})} = G_{\mathrm{chem}}^{\mathrm{dis\_(S)}} + \Delta G^{(\mathrm{ord})}\left(y_i^{(l)}\right) . \tag{5}$$

To describe the ordered phase, two or more sublattices are used. For example, a binary alloy using four sublattices can be expressed as:

$$(\mathrm{TM, Pt})_{0.25}(\mathrm{TM, Pt})_{0.25}(\mathrm{TM, Pt})_{0.25}(\mathrm{TM, Pt})_{0.25} , \tag{6}$$

$$c_i = 0.25\sum_{l=1}^{4} y_i^{(l)} , \quad i \le n-1 , \tag{7}$$

where, $y_i^{(l)}$ is the site fraction of constituent i on sublattice l. The more detailed form of $\Delta G^{(\mathrm{ord})}$ is presented in Ref. (11). Here, to reduce the number of field variables, we adopted a three-component LRO parameter, $\mathbf{S}$,[12] defined as follows:

$$\mathbf{S} = \begin{pmatrix} s_1 \\ s_2 \\ s_3 \end{pmatrix} = \frac{1}{2}\begin{pmatrix} s_{1,\mathrm{Pt}} - s_{1,\mathrm{TM}} \\ s_{2,\mathrm{Pt}} - s_{2,\mathrm{TM}} \\ s_{3,\mathrm{Pt}} - s_{3,\mathrm{TM}} \end{pmatrix} \text{ with}$$

$$\begin{pmatrix} s_{1,i} \\ s_{2,i} \\ s_{3,i} \end{pmatrix} = \frac{1}{2}\begin{pmatrix} y_i^{(1)} + y_i^{(2)} - y_i^{(3)} - y_i^{(4)} \\ y_i^{(1)} - y_i^{(2)} - y_i^{(3)} + y_i^{(4)} \\ y_i^{(1)} - y_i^{(2)} + y_i^{(3)} - y_i^{(4)} \end{pmatrix} , \ i = \mathrm{Pt\ or\ TM} . \tag{8}$$

$\mathbf{S} = (s_1, s_2, s_3)$ takes on the values (±1, 0, 0), (0, ±1, 0) and (0, 0, ±1) for the complete $L1_0$ and $L1_1$ ordered phases, and (±0.5, ±0.5, ±0.5) for the complete $L1_2$ ordered phase. The interaction parameters between the metallic elements are evaluated by the calculation of phase diagram (CALPHAD) method.[11] In this method, the interaction parameters are determined to appropriately reproduce the experimentally observed or theoretically estimated phase boundaries and thermodynamic properties. Recently, thermodynamic assessments have been carried out for a number of alloy systems. Thus, the phase-field method can be applied to numerous alloy systems in combination with the CALPHAD database. The coefficients $L_{12}^{(k)}$ and $\Delta G^{(\mathrm{ord})}$, shown in Eqs. (4) and (5), are provided as polynomial equations in terms of atomic concentrations based on thermodynamic assessments of the Cr-Pt,[13] Fe-Pt,[14] Co-Pt,[15] Ni-Pt,[16] Cu-Pt,[17] Pd-Pt,[18] Ir-Pt,[19] and Au-Pt[20] binary systems. The coefficient $L_{in}^{(k)}$ is a pair-wise interaction parameter between alloy element i and a vacancy, and it is defined as follows:

$$L_{in}^{(k)} = \Delta H_{\mathrm{f},i}^{(k)} - T\Delta S_{\mathrm{f}} , \ i \le n-1 , \ k = \mathrm{S\ or\ L} , \tag{9}$$

where $\Delta H_{\mathrm{f},i}^{(k)}$ and ΔS_{f} are the enthalpy and entropy of mono-vacancy formation, respectively. The ΔS_{f} value can be expressed as $1.32R$, which was originally used for platinum.[21] The coefficients $\Delta H_{\mathrm{f},i}^{(k)}$ in Eq. (9) and $\kappa_{i=n}$ in Eq. (1) are calculated simultaneously as explained below.

If all of the thermodynamic fields are not spatially uniform, then the gradient energy must be supplemented to account for the energetic interactions between the system and its surrounding. In this approach, the thermodynamic variables are assumed to change smoothly from one phase or domain to another.[22] By introducing the gradient energy term, phase-field models can overcome the computational difficulty of tracking a moving boundary, which is usually diffused in real physical systems. The gradient energy coefficient, κ, can be determined from the relationship between the free energy change across the interface, Δf, and surface energy, γ,[23,24] as follows:

$$\gamma = \int_{c_{\mathrm{B}}}^{c_{\mathrm{A}}} \frac{\sqrt{2\kappa\Delta f(c)}}{V_{\mathrm{m}}} dc , \tag{10}$$

where the variables c_{A} and c_{B} denote the equilibrium concentrations of the two phases, and V_{m} is the molar volume. The thickness of the interfacial layer, Δd, can be approximated by the following equation from the concentration gradient when Δf is maximized:

$$\Delta d = (c_{\mathrm{A}} - c_{\mathrm{B}})/(\mathrm{d}c/\mathrm{d}x) = (c_{\mathrm{A}} - c_{\mathrm{B}})\sqrt{\kappa/2\Delta f_{\max}} . \tag{11}$$

Equation (11) indicates that the coefficient κ is also determined using Δf and Δd. In the case of the condensed matter-vapor interface, Δf is governed by the $L_{in}^{(k)}$ value. The coefficient κ_n for the alloy-vapor interface was defined as a linear combination of the κ_{in} values, where κ_{in} is defined as the gradient coefficient for the pure element (i)-vapor interface.[10] Therefore, $\Delta H_{\mathrm{f},i}^{(k)}$ and κ_{in} need to be determined to reproduce the γ and Δd values of the pure metal element i. The γ value was defined as the (111) surface energy of the fcc structure.[25,26] The Δd value for the solid phase was set at 3.0×10^{-10} m, which is consistent with

the results of molecular dynamics simulations.[27] In the case of the solid-liquid interface, W and κ_θ were determined using the solid-liquid interface energy and Δd (where Δd was assumed to be approximately equal to the thickness of the solid-vapor interface). The κ_s value for the ordered-disordered phase interface was determined to reproduce the width of the anti-phase boundary (APB) and the $\Delta f_{\max}$ value using Eq. (11). Here, the $\Delta f_{\max}$ value corresponds to the absolute value of $\Delta G^{(\mathrm{ord})}$. The value of Δd used was 1.0×10^{-9} m, which was close to the experimentally observed value of approximately 1.38×10^{-9} m for FePt.[28] The value of κ_i ($i < n$), which pertains to the solid-solid interface between two coexisting phases is determined by using the interfacial energy heights estimated from the CALPHAD data and assuming a solid-solid interface width of 1×10^{-9} m.

2. 2 Phase-field Equations

The conservative temporal evolution of the atomic concentration was calculated using a Cahn-Hilliard type equation,[29] which can be represented as follows:

$$\frac{\partial c_i}{\partial t} = \nabla \cdot \left[\sum_{j=1}^{n-1} M_{ij} \nabla \left(\frac{\delta G_{\mathrm{sys}}}{\delta c_j} \right) \right], \; i \le n-1 . \tag{12}$$

The coefficient M_{ij}, which is the mobility of component i owing to the gradient of the functional derivative of G_{sys} with respect to the concentration of component j, is expressible as:[30]

$$M_{ii} = c_i(1-c_i)D/RT \;\text{ and }\; M_{ij} = M_{ji} = -c_i c_j D/RT , \tag{13}$$

where D is the self-diffusion coefficient. The temporal evolution of the concentration of each component can be calculated under the condition that the total value of the concentration variable for each grid point is 1. The non-conservative temporal evolution of the ordered phase-disordered A1 fcc phase and the solid-liquid phase within a nanoparticle are calculated using Allen-Cahn type equations,[31] which can be represented as follows:

$$\frac{\partial s_i}{\partial t} = -L_s \frac{\delta G_{\mathrm{sys}}}{\delta s_i}, \;\; i \le 3 , \tag{14}$$

$$\frac{\partial \theta}{\partial t} = -L_\theta \frac{\delta G_{\mathrm{sys}}}{\delta \theta} , \tag{15}$$

where L_s and L_θ denote the mobility of the ordered-disordered and solid-liquid phase interfaces, respectively.

A numerical calculation of the one-dimensional problem along the radial direction of a nanoparticle was performed. The finite volume method was used to solve the partial differential equations (Eqs. (12), (14), and (15)). In the initial state, the same alloy composition ratio was used for all the areas inside the particle. In the present study, we focused on obtaining the steady-state microstructure. Therefore, the simulated time step was varied according to the flux of the atomic concentration in order to reduce the simulation time. The grid spacing at each grid point was updated at each time step. The boundary conditions at $r = 0$ and $r = l$ were chosen such that the spatial derivatives of the field variables were zero. In the external region of the particle, only vaporized atomic elements were present, *i.e.*, the atmosphere was inert. Detailed explanations of the numerical calculation scheme for a binary-alloy nanoparticle utilizing the phase-field method are presented in Refs. (9) and (10).

3. Results and Discussion

3. 1 Phase Transformations

The accuracy of this method for the phase transformations, which affect the degree of surface segregation, was compared with experimental and other simulation results. First, the radial distribution of the long-range order parameter was evaluated for the binary alloys exhibiting the order-disorder phase transition. **Figure 2** shows the simulated particle size dependence of the $L1_0$ ordering averaged over a single FePt particle at 973.15 K. The degree of $L1_0$ ordering decreases as the particle size decreases. Since the curvature of the ordered-disordered interface increases with decreasing particle size, the gradient energy term, κ_s, causes this phase transformation primarily in the direction that decreases the interfacial energy of the ordered-disordered phases. When the APB width was assumed to be 1.0 nm, in accordance with the experimental results described in Sec. 2.1, the calculated gradation of the degree of $L1_0$ ordering was consistent with experimental results reported in the literature.[32-34] This indicates that the present phase-field model is sufficiently accurate in describing the order-disorder phase transition within a nanoparticle.

Another important feature was the particle size dependence of the solid-liquid transition temperature.

Figure 3 plots the simulated phase boundary between the solid and liquid phases of the FePt nanoparticle against the holding temperature and the particle size. When the particle diameter was at the nanometer scale, the influence of the solid-liquid interfacial energy of the particle on its chemical potential was significant through κ_θ. Therefore, the liquid phase is more likely to form at the particle surface even when the holding temperature is lower than the melting point of the bulk material. Furthermore, when the stability of the solid phase of the particle interior is in balance with the solid-liquid interfacial energy near the particle surface, a kind of core-shell structure is formed in the particle because the particle surface melts; this is known as surface pre-melting.[35] In Fig. 3, the open circles denote completely melted particles and filled circles denote partially melted particles. The crossover from filled to open circles indicates the simulated transition temperature of the solid-liquid phases. The decrease in transition temperature in particles less than 10 nm in diameter was more marked than that in larger particles. Figure 3 also shows the results from the classical theoretical model (so-called Pawlow's model).[36] The simulated phase boundary between the solid and liquid phases was at a slightly lower temperature than that obtained with the classical model. We attributed the discrepancy in phase boundary temperature to surface pre-melting. The Ag nanoparticle study of molecular dynamics[37] corroborates this conclusion.

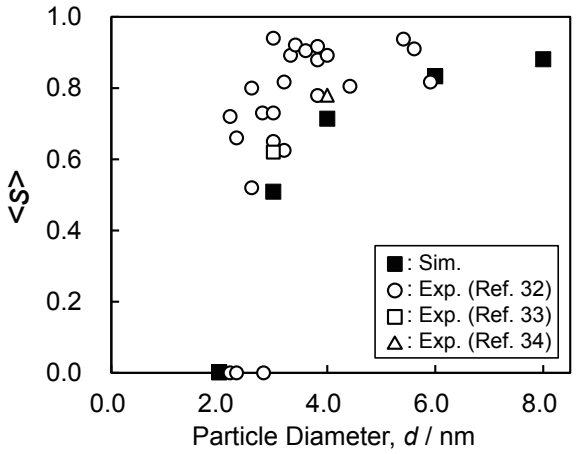

Fig. 2 Comparison of the dependence of $L1_0$ ordering of the FePt particles on particle size with experimental results.

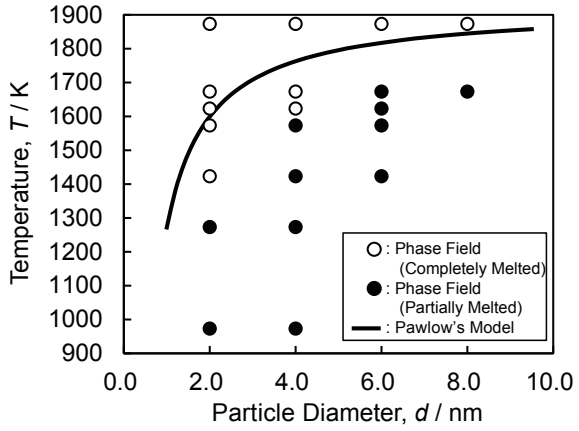

Fig. 3 Phases of the FePt particles calculated with respect to the particle size (circles), plotted together with the phase boundaries predicted by Pawlow's model[36] (solid line).

3. 2 Surface Segregation

Figure 4 shows the radial distributions of the atomic concentrations (c_{Pt}, c_{TM} and c_{Pt+TM}) and the values of |**S**| for the ordered-disordered phase of nanoparticles with a diameter of 3 nm at 973.15 K. To simplify the description of the interatomic interaction and the surface energy, the calculation was performed under conditions that ignored the presence of the liquid phase. The compositional ratio of Pt to TM was 1:1. The region where the summation of the concentration of the component elements, excluding the vacancy (indicated by the black solid line), varies from 0 to 1 corresponds to the particle surface. The difference in the composition ratios and the surface-segregated element was determined from the distributions of c_{Pt} and c_{TM} with respect to the horizontal axis in Fig. 4. In the case of FePt and CoPt, no significant surface segregation occurred. In contrast, the surfaces of IrPt and AuPt were composed of one of the two alloy component elements. In the case of CrPt, NiPt, CuPt and PdPt, the concentration of one element was slightly higher, while both elements were still present on the particle surface. These simulated results of the surface enrichment of the alloy element were in fairly good agreement with those of the previously reported Monte Carlo simulations, with the exception of NiPt.[10] In the case of NiPt, the surface energy difference between the two elements was small. Thus, surface enrichment is presumably governed by other factors, such as atomic size mismatch, that are not considered in this model.

To quantify the extent of surface segregation, the expression $(\Sigma c_{Pt} - \Sigma c_{TM}) / \Sigma(c_{Pt} + c_{TM})$ is evaluated for the shell region of the nanoparticle, *i.e.*, $r \geq (d/2 - 0.5)$, which corresponds to the surface shell of the nanoparticle (d is the particle diameter in nm). A positive or negative value corresponds to Pt or TM segregation, respectively. The values obtained are plotted against the surface energy difference in **Fig. 5**. The coefficients γ'_{Pt} and γ'_{TM} are defined as γ_{Pt} and γ_{TM} multiplied by the atomic surface areas of their (111) crystal planes, respectively. The difference in surface energy between the two metallic elements acted as a driving force for surface segregation in these alloy particles. Figure 5 shows that the alloy element with

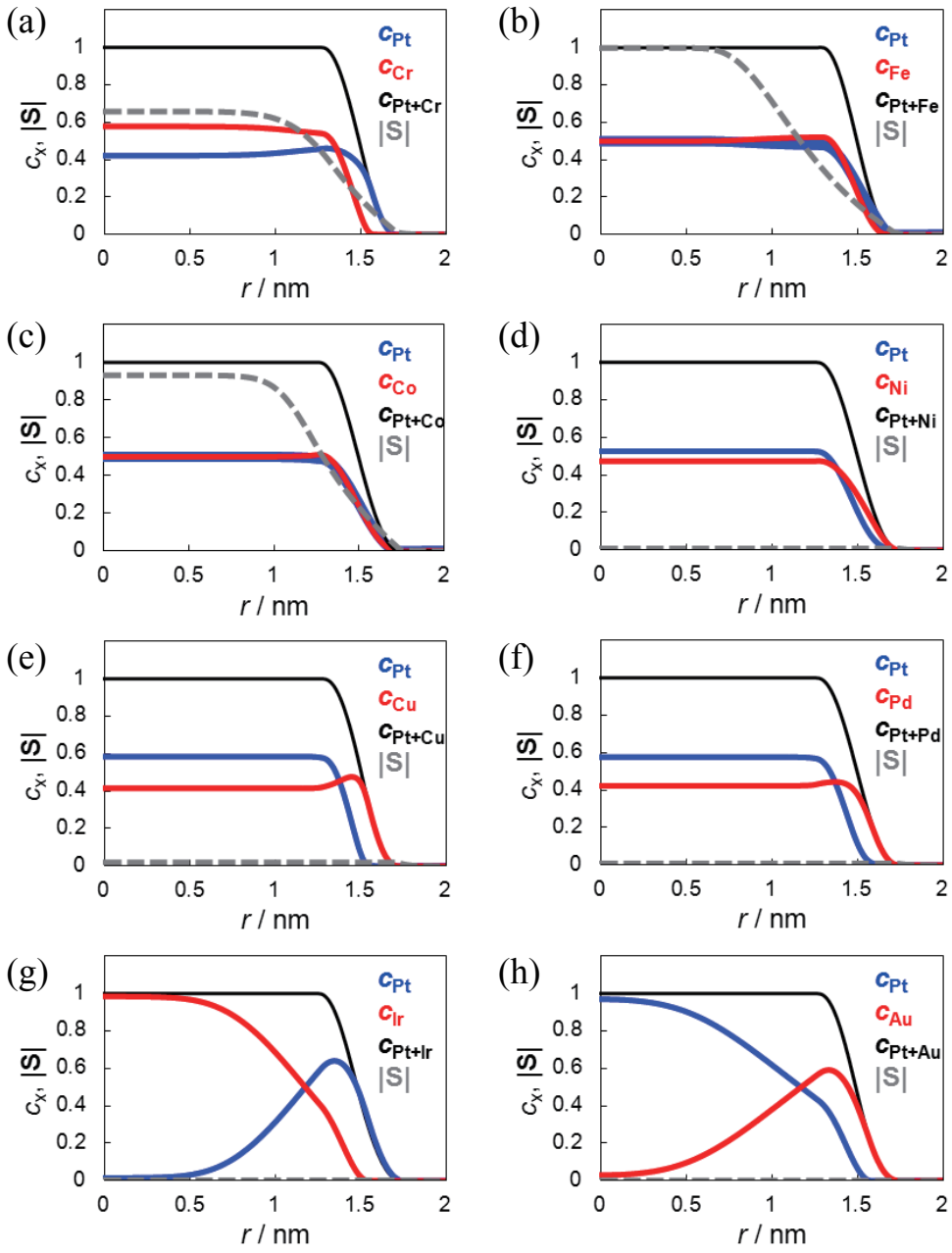

Fig. 4 Radial distribution of the mole fraction of each atom, c_x, and the long-range ordering parameter, |**S**|, within (a) CrPt, (b) FePt, (c) CoPt, (d) NiPt, (e) CuPt, (f) PdPt, (g) IrPt and (h) AuPt nanoparticles with a diameter of 3 nm at 973.15 K. The horizontal axis denotes the distance from the particle center. Except for CrPt particle, the |**S**| values of 0 and 1 correspond to the disordered phase and $L1_0$ (or $L1_1$) ordered phase, respectively. In the case of CrPt particle, the |**S**| values of 0 and 0.866 correspond to the disordered phase and $L1_2$ ordered phase, respectively.

the lower surface energy tended to segregate near the surface. The surface segregation did not only depend on the alloy surface energies and the particle volume. Rather, as shown in Fig. 5, the effect of the particle diameter on the degree of segregation also varied with the combination of alloying elements. In the case of AuPt and IrPt, significant surface segregation was triggered by the large difference in surface energy. On the other hand, FePt particles did not exhibit significant surface segregation, although the absolute difference in surface energy between Fe and Pt was almost identical to that between Cu and Pt. Thus, because the degrees of segregation for all examined alloy nanoparticles with the same diameter did not fit on the same straight line, it appears that surface segregation was not governed by the surface energy difference alone. Other contributing factors may include an attractive (repulsive) interaction between the two elements in the alloy particle, which would suppress (promote) surface segregation.

In order to help visualize the general characteristics of the surface segregation, information regarding the degree of segregation was plotted as a two-dimensional map of the free energy of mixing of the binary alloy vs. the surface energy difference using the CALPHAD data, as shown in **Fig. 6**. For all alloys except IrPt and AuPt, the free energies of mixing with respect to the vertical axis in Fig. 6 were evaluated as deviations from the linear combinations of the free energies of the two pure end products of the solutions. In the case of IrPt and AuPt, the mixing energies were evaluated as deviations from the tie-lines that connect the equilibrium compositions of the Pt-rich and Ir-rich (or Au-rich) phases. The surface energy difference on the horizontal axis is the same as that of Fig. 5. The degree of surface segregation in the alloy particles is expressed by the numerical values shown in parentheses.

In Fig. 6, an alloy with a large negative value on the vertical axis means that the solid solution state, including the ordered phase, is stable. For example, no segregation occurs in the FePt particle despite the surface energy difference, because of the effect of this large mixing energy. In the case of IrPt and AuPt, the mixing energy has a positive value on the vertical axis, which indicates that the solid solution is unstable and that decomposition into a TM- or Pt-rich phase has occurred. Here, the phase decomposition triggered by surface segregation is promoted and the surface layer is occupied by one of the two elements. In the case of other binary systems such as CrPt, NiPt, CuPt, and PdPt, the surface-segregated species is determined by the surface energy difference, and the degree of surface

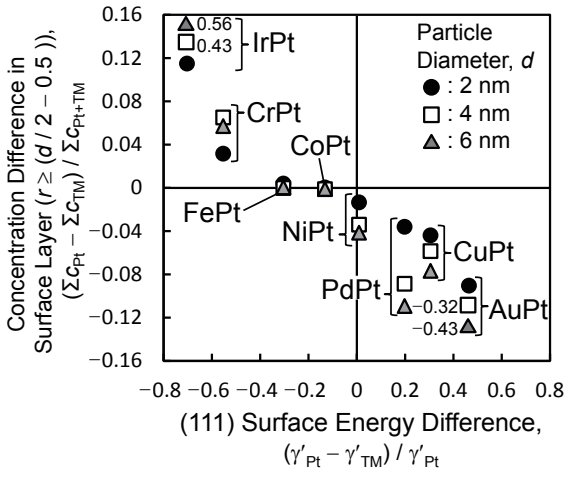

Fig. 5 Relationship between the degree of surface segregation and surface energy difference. Positive values on the vertical axis indicate segregation of Pt on the particle surface; positive values on the horizontal axis indicate that the surface energy of Pt was larger than that of the transition metal.

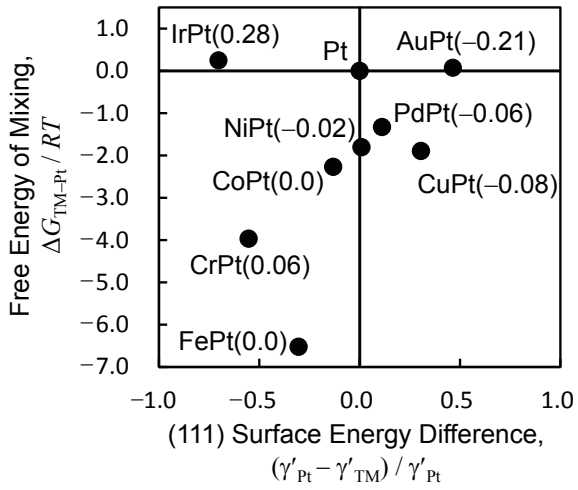

Fig. 6 Trend of surface atomic segregation of Pt-based binary nanoparticles. The number in parentheses following the name of each alloy element is the value calculated using the equation $(\Sigma c_{Pt} - \Sigma c_{TM}) / \Sigma(c_{Pt} + c_{TM})$ for the region where $r \geq (d/2 - 0.5)$ (d is the particle diameter in nm), which corresponds to the surface shell of the nanoparticle. Numerical calculation results were obtained for a particle with a diameter of 3 nm at 973.15 K.

segregation is determined by the balance between the surface energy and the chemical interaction between the atomic components. Furthermore, the degree of surface segregation in the binary alloys located in the third quadrant of this map (such as CrPt, FePt, and CoPt) is slightly smaller than that of the binary alloys in the fourth quadrant (such as NiPt, CuPt, and PdPt). In the case of CrPt, FePt, and CoPt, the ordered phase is stable. If an ordered phase is generated, the compositional shift is suppressed more strongly because the energy change as a function of the deviation of the composition from a 1:1 composition is more significant. Therefore, the asymmetry behavior in the degree of surface segregation with respect to the horizontal axis presumably results from the formation of an ordered phase. Moreover, the degree of ordering increases as the particle diameter increases (see Fig. 2). Thus, in order to reduce excessive surface segregation and prevent instability in the alloy system, it is possible to take advantage of the formation of ordered phases by increasing the particle size and performing a heat treatment at an appropriate temperature.

4. Conclusion

The phase-field method was applied to nanometer-sized electrode materials in the context of improving the performance of a cathode electrocatalyst. The radial distributions of the phase transformations and surface segregation in TM-Pt binary alloy nanoparticles were examined as functions of the input values of alloy composition, particle diameter, and temperature. The results revealed that the compositional variation within individual particles depended on the balance between interatomic interactions within the particle and the surface energy. The specific equilibrium points varied significantly with the combination of TM-Pt alloys. Therefore, the internal structure of the alloy nanoparticles may often differ from that of the nominal bulk state, because the variability in surface energy caused by the particle size distribution influences the thermal equilibrium microstructure of the nanoparticles. In order to reduce excessive surface segregation and prevent instability in the alloy system, it is possible to take advantage of the formation of ordered phases. The present findings demonstrate that phase-field modeling studies can elucidate the driving forces behind nanostructure formation.

References

(1) Chen, L. Q., “Phase-field Models for Microstructure Evolution”, *Ann. Rev. Mater. Res*., Vol. 32 (2002), pp. 113-140.
(2) Koyama, T., “Phase-field Modeling of Microstructure Evolutions in Magnetic Materials”, *Sci. Technol. Adv. Mater*., Vol. 9 (2008), 013006.
(3) Mehta, V. and Cooper, J. S., “Review and Analysis of PEM Fuel Cell Design and Manufacturing”, *J. Power Sources*, Vol. 114, No. 1 (2003), pp. 32-53.
(4) Yamakawa, S., “Phase-field Models for Microstructural Characterization of Electrode Materials”, *Dr. Thesis, Nagoya Institute of Technology* (2014), p. 4.
(5) Debe, M. K., “Electrocatalyst Approaches and Challenges for Automotive Fuel Cells”, *Nature*, Vol. 486, No. 7401 (2012), pp. 43-51.
(6) Alloyeau, D., Prévot, G., Bouar, Y. L., Oikawa, T., Langlois, C., Loiseau, A. and Ricolleau, C., “Ostwald Ripening in Nanoalloys: When Thermodynamics Drives a Size-dependent Particle Composition”, *Phys. Rev. Lett*., Vol. 105 (2010), 255901.
(7) Ferrando, R., Jellinek, J. and Johnston, R. L., “Nanoalloys: from Theory to Applications of Alloy Clusters and Nanoparticles”, *Chem. Rev*., Vol. 108, No. 3 (2008), pp. 845-910.
(8) Stamenkovic, V. R., Mun, B. S., Mayrhofer, K. J. J., Ross, P. N. and Markovic, N. M., “Effect of Surface Composition on Electronic Structure, Stability, and Electrocatalytic Properties of Pt-transition Metal Alloys: Pt-skin versus Pt-skeleton Surfaces”, *J. Am. Chem. Soc*., Vol. 128, No. 27 (2006), pp. 8813-8819.
(9) Yamakawa, S., Asahi, R. and Koyama, T., “Phase-field Modeling of Phase Transformations in Platinum-based Alloy Nanoparticles”, *Mater. Trans*., Vol. 54, No. 8 (2013), pp. 1242-1249.
(10) Yamakawa, S., Asahi, R. and Koyama, T., “Surface Segregations in Platinum-based Alloy Nanoparticles”, *Surface Science*, Vol. 622, No. 4 (2014), pp. 65-70.
(11) Lukas, H. L., Fries, S. G. and Sundman, B., *Computational Thermodynamics − The Calphad Method* (2007), 324p., Cambridge Univ. Press.
(12) Binder, K., Lebowitz, J. L., Phani, M. K. and Kalos, M. H., “Monte Carlo Study of the Phase Diagrams of Binary Alloys with Face Centered Cubic Lattice Structure”, *Acta Metall*., Vol. 29, No. 9 (1981), pp. 1655-1665.
(13) Preußner, J., Prins, S., Völkl, R., Liu, Z.-K. and Glatzel, U., “Determination of Phases in the System Chromium-platinum (Cr-Pt) and Thermodynamic Calculations”, *Mat. Sci. Eng. A*, Vol. 510-511 (2009), pp. 322-327.
(14) Fredriksson, P. and Sundman, B., “A Thermodynamic Assessment of the Fe-Pt System”, *Calphad*, Vol. 25, No. 4 (2001), pp. 535-548.
(15) Kim, D., Saal, J. E., Zhou, L., Shang, S., Du, Y. and Liu, Z.-K., “Thermodynamic Modeling of Fcc

Order/disorder Transformations in the Co-Pt System", *Calphad*, Vol. 35, No. 3 (2011), pp. 323-330.
(16) Lu, X.-G., Sundman, B. and Ågren, J., "Thermodynamic Assessments of the Ni-Pt and Al-Ni-Pt Systems", *Calphad* , Vol. 33, No. 3 (2009), pp. 450-456.
(17) Abe, T., Sundman, B. and Onodera, H., "Thermodynamic Assessment of the Cu-Pt System", *J. Phase Equilib. Diffus*., Vol. 27, No. 1 (2006), pp. 5-13.
(18) Turchi, P. E. A., Drchal, V. and Kudrnovský, J., "Stability and Ordering Properties of Fcc Alloys Based on Rh, Ir, Pd, and Pt", *Phys. Rev. B*, Vol. 74 (2006), 064202.
(19) Abe, T., *Zairyou Sekkei Keisan Kougaku; Keisan Netsurikigakuhen* (in Japanese) (2011), 192p., Uchida Rokakuho Publishing, Tokyo.
(20) Grolier, V. and Schmid-Fetzer, R., "Experimental Study of Au-Pt-Sn Phase Equilibria and Thermodynamic Assessment of the Au-Pt and Au-Pt-Sn Systems", *J. Electron. Mater*., Vol. 37, No. 3 (2008), pp. 264-278.
(21) Arblaster, J. W., "Crystallographic Properties of Platinum", *Platinum Met. Rev*., Vol. 50, No. 3 (2006), pp. 118-119.
(22) Koyama, T., *Zairyou Sekkei Keisan Kougaku*; *Keisan Soshikigakuhen* (in Japanese) (2011), 137p., Uchida Rokakuho Publishing, Tokyo.
(23) Cahn, J. W. and Hilliard, J. E., "Free Energy of a Nonuniform System. I. Interfacial Free Energy", *J. Chem. Phys*., Vol. 28, No. 2 (1958), pp. 258-267.
(24) Saito, Y., *Soshikikeisei to Kakusan Houteishiki* (in Japanese) (2000), 171p., Corona Publishing Co., Tokyo.
(25) Wen, Y. N. and Zhang, J. M., "Surface Energy Calculation of the Fcc Metals by Using the MAEAM", *Solid State Commun*., Vol. 144, No. 3-4 (2007), pp. 163-167.
(26) Dannenberg, A., Gruner, M. E., Hucht, A. and Entel, P., "Surface Energies of Stoichiometric FePt and CoPt Alloys and Their Implications for Nanoparticle Morphologies", *Phys. Rev. B*, Vol. 80 (2009), 245438.
(27) Chui, Y. H. and Chan, K. Y., "Analyses of Surface and Core Atoms in a Platinum Nanoparticle", *Phys. Chem. Chem. Phys*., Vol. 5, No. 13 (2003), pp. 2869-2874.
(28) Watanabe, M., Masumoto, T., Ping, D. H. and Hono, K., "Microstructure and Magnetic Properties of FePt-Al-O Granular Thin Films", *Appl. Phys. Lett*., Vol. 76, No. 26 (2000), pp. 3971-3973.
(29) Cahn, J. W., "Phase Separation by Spinodal Decomposition in Isotropic Systems", *J. Chem. Phys*., Vol. 42, No. 1 (1965), pp. 93-99.
(30) Villanueva, W., Grönhagen, K., Amberg, G. and Ågren, J., "Multicomponent and Multiphase Modeling and Simulation of Reactive Wetting", *Phys. Rev. E*, Vol. 77 (2008), 056313.
(31) Allen, S. M. and Cahn, J. W., "A Microscopic Theory for Antiphase Boundary Motion and Its Application to Antiphase Domain Coarsening", *Acta Metall*., Vol. 27, No. 6 (1979), pp. 1085-1095.
(32) Miyazaki, T., Kitakami, O., Okamoto, S., Shimada, Y., Akase, Z., Murakami, Y., Shindo, D., Takahashi, Y. K. and Hono, K., "Size Effect on the Ordering of $L1_0$ FePt Nanoparticles", *Phys. Rev. B*, Vol. 72 (2005), 144419.
(33) Rong, C. B., Poudyal, N., Chaubey, G. S., Nandwana, V., Skomski, R., Wu, Y. Q., Kramer, M. J. and Liu, J. P., "Structural Phase Transition and Ferromagnetism in Monodisperse 3 nm FePt Particles", *J. Appl. Phys*., Vol. 102, No. 4 (2007), 043913.
(34) Rong, C. B., Li, D., Nandwana, V., Poudyal, N., Ding, Y., Wang, Z. L., Zeng, H. and Liu, J. P., "Size-dependent Chemical and Magnetic Ordering in $L1_0$-FePt Nanoparticles", *Adv. Mater*., Vol. 18, No. 22 (2006), pp. 2984-2988.
(35) Wang, Z. L., Petroski, J. M., Green, T. C. and El-Sayed, M. A., "Shape Transformation and Surface Melting of Cubic and Tetrahedral Platinum Nanocrystals", *J. Phys. Chem. B*, Vol. 102, No. 32 (1998), pp. 6145-6151.
(36) Barybin, A. and Shapovalov, V., "Modification of Pawlow's Thermodynamical Model for the Melting of Small Single-component Particles", *J. Appl. Phys*., Vol. 109 (2011), 034303.
(37) Zhao, S., Wang, S. and Ye, H., "Size-dependent Melting Properties of Free Silver Nanoclusters", *J. Phys. Soc. Jpn*., Vol. 70, No. 10 (2001), pp. 2953-2957.

Shunsuke Yamakawa
Research Field:
- Computational Materials Science

Academic Degree: Dr.Eng.
Academic Society:
- The Japan Institute of Metals and Materials

Ryoji Asahi
Research Field:
- Computational Materials Design of Functional Materials

Academic Degree: Ph.D.
Academic Societies:
- The Japan Society of Applied Physics
- American Physical Society
- The Japan Institute of Metals

Awards:
- Advanced Technology Award, Japan Fine Ceramics Association, 2003
- Corporate Environmental Achievement Award, The American Ceramic Society, 2006
- Technical Development Award, The Chemical Society of Japan, 2006

Toshiyuki Koyama*
Research Fields:
- Education
- Materials Science and Engineering

Academic Degree: Dr.Eng.
Academic Societies:
- The Japan Institute of Metals and Materials
- The Iron and Steel Institute of Japan
- The Japan Society of Mechanical Engineers
- The Japan Society for Computational Engineering and Science
- The Minerals, Metals and Materials Society
- Materials Research Society

Awards:
- The Japan Institute of Metals and Materials Young Researcher Award, 1991
- The Japan Institute of Metals and Materials Meritorious Award, 2006
- Materia Japan Award for Science and Technology, 2006
- Scientific Achievement Commemorative Prize (Nishiyama Commemorative Prize), 2008
- Materia Japan Award for Education, 2012

* Nagoya Institute of Technology

